Examining Copper Lead Surface Alloys as Potential Catalysts for the Electrochemical Carbon Dioxide Reduction

Oliver Kratz[†] and Axel Groß[*,†]

†*Institute of Theoretical Chemistry, Ulm University, Oberberghof 7, 89081 Ulm, Germany*

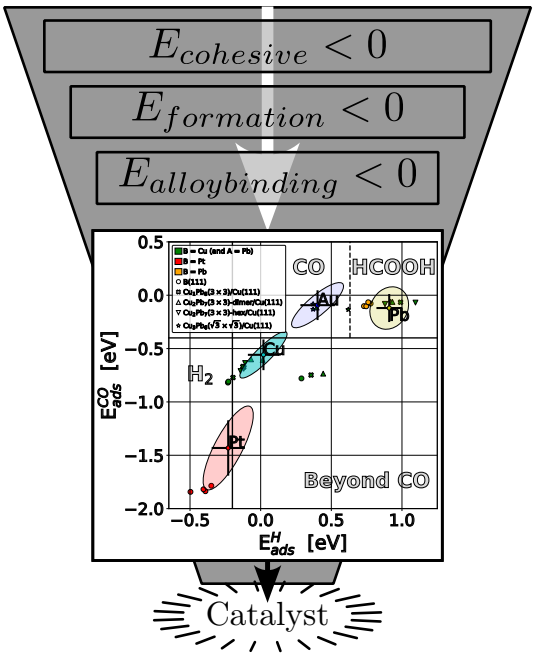
‡*Helmholtz Institute Ulm (HIU) for Electrochemical Energy Storage, Helmholtzstraße 11, 89081 Ulm, Germany*

E-mail: axel.gross@uni-ulm.de

Abstract

The conversion of carbon dioxide into useful or environmentally benign chemicals is currently of great interest to reduce greenhouse gas emissions. Yet in spite of numerous efforts effective CO_2 conversion still presents a considerable challenge. One of the most promising catalysts for CO_2 conversion to hydrocarbons is copper. In this computational study based on density functional theory we have addressed bimetallic PbCu catalysts to elucidate whether there are synergistic catalytic effects through the alloying of Cu with Pb, as suggested experimentally. Using a well-established descriptor for the catalytic activity based on hydrogen and CO adsorption energies, we analyzed the potential catalytic activity of PbCu surface alloys on copper. The computational results confirm that through a combination of strain and ligand effects these surface alloys can act as favorable catalysts for valuable hydrocarbons.

Table of Contents Graphics



Introduction

Reducing carbon dioxide emissions is a central objective in climate change mitigation.[1] However, this reduction alone will not be sufficient to reach the climate goals, in addition CO_2 also needs to be converted into useful or at least harmless products.[2,3] Furthermore, some societally and economically important processes such as waste incineration or cement production will continue to produce carbon dioxide.[4,5] More generally, carbon dioxide needs to become a feedstock in the strive for a circular economy. This means that there is a need for carbon dioxide to be chemically converted into a plethora of compounds.

Regarding carbon dioxide removal (CDR) technologies, compounds like oxalate or formic acid are desirable compounds as they allow the save and energetically inexpensive storage of carbon.[2] On the other hand, for industrial purposes, CO_2 can also be converted to products such as carbon monoxide and hydrocarbons. Carbon monoxide can be used, e.g., for the production of phosgene.[6] Complex hydrocarbons can be used, e.g., as synthetic fuels or as the basis for commodity chemicals.[7] Thus, the conversion of carbon dioxide into ei-

ther value added products for industrial purposes or sink products for CDR has become of increasing interest to combat climate change.[2,3,8,9] Both paths require efficient and ideally cheap catalysts for CO_2 reduction.[2,10,11] One way to chemically convert carbon dioxide is electrochemical reduction. This has motivated numerous research activities, but it is fair to say that an ideal CO_2 reduction reaction (CO2RR) catalyst is still missing.[12–17]

Although the ideal catalyst remains elusive, there are promising experimental results such as waste-derived copper-lead catalysts promoting CO as main product or a cerium-added metal alloy facilitating solid carbon production for electrocatalytic CO_2 reduction.[18,19] It is certainly fair to say, for improving upon CO2RR catalysts a robust theoretical understanding of structure-reactivity relations can be very beneficial.[20] Insight in these relations is important as due to the inherent complexity of the CO2RR, it is still a challenge to adequately describe the corresponding catalytic processes on a quantum chemical level.[21–27]

To reduce this complexity of catalytic reactions, descriptors can be used. Descriptors reflect correlations between material properties and desired or undesired functionality of these materials.[28] The identification of descriptors can considerably accelerate the search for materials with desired functional or multi-functional properties because in a first step only materials with the optimized descriptor need to be detected.[29–33] In the field of CO_2 conversion, Bagger *et al.* identified descriptors for the selectivity of the electrochemeical CO2RR on transition metal cathodes/catalysts.[34] They used binding energies of possible intermediates in the CO2RR as descriptors for the main product of the reaction which was derived from experiments by Hori *et al.*[35] As a result they found that using the individual adsorption energies of (atomic) hydrogen and carbon monoxide on the fcc (111) surface of transition metals, the metals could be clustered into four main product groups. These main products are H_2, CO, HCOOH, and Beyond CO where Beyond CO stands for any hydrocarbon or alcohol. Consequently, the adsorption energies of hydrogen and carbon monoxide can be used as descriptors for these four product groups.

In our present work, we focussed on the catalytic activity of copper-lead alloys regard-

ing CO_2 reduction. Among transition metals as catalysts, copper stands out, as it is the only (pure) metal that is considered to be able to catalyze the production of hydrocarbons from CO_2.[34] This makes the idea enticing of slightly modifying copper surfaces to possibly get a more efficient catalyst. In fact, experimental studies have already shown that CuPb bimetallic catalysts can exhibit favorable catalytic properties with respect to carbon dioxide reduction.[18,36–39]

Our work first re-analyzes the approach from Bagger *et al.*[34] and proposes a workflow for systematically examining the catalytic properties of surface alloys. We have then used this workflow to determine the suitability of copper lead surface alloys for catalysing the electrochemical CO2RR. The workflow included the determination of hydrogen and CO adsorption energies on CuPb/Cu(111) surface alloys performing first-principles electronic structure calculations. The adsorption energies on the bimetallic catalysts have been analyzed using the concept of strain and ligand effects. Our work suggests that Pb doping of Cu catalysts can with certain caveats improve the performance of the Cu catalysts.

Theoretical and computational approach

Quantum chemical calculations

All calculations were performed in the spin-unpolarized formalism using VASP 6.3.0 (**V**ienna **A**b initio **S**imulation **P**ackage).[40–43] Spin-unpolarized calculations are sufficient as carbon monoxide is a closed shell system, hydrogen looses its electron fully to the electron sea of the metal and both copper and lead or not magnetic. Nevertheless, adequacy of spin-unpolarized calculations was confirmed on a subset of all structures (section S1 of the Supporting Information). Geometries were generated with the ASE (**A**tomic **S**imulation **E**nvironment) Python package.[44] The supercell consisted of a five-layer 3×3 slab of the (111) fcc surface with 15 Å vacuum. The two bottom layers were fixed.

Van der Waals (VdW) interactions were corrected using the zero-damping DFT-D3

method of Grimme.[45,46] To mitigate the known overestimation of metal–metal interactions,[47–49] VdW interactions between identical or dopant metal atoms were disabled. Additionally, to reduce overestimation of long-range dispersion on metal surfaces,[50] VdW interactions between the adsorbate and the bottom four layers were excluded.

A plane-wave cutoff of 600 eV with Gaussian smearing and fixed cell shape was used. Structures were relaxed until all forces were below 0.01 eVÅ^{-1}. The standard pseudo potentials after[42] were used, which treat $3d^{10}4s^1$ electrons for copper and $6s^26p^2$ electrons for lead as valance electrons. A Monkhorst–Pack sampling[51,52] with $6 \times 6 \times 1$ k-point grid was employed. For the density of states calculations the pseudo potential of lead was swapped to the pseudo potential treating $5d^{10}6s^26p^2$ as valance electrons and consecutive Monkhorst–Pack sampling grids of $11 \times 11 \times 1$ and $21 \times 21 \times 1$ were used. All calculations employed the revised Perdew–Burke–Ernzerhof (RPBE) functional within the GGA framework, combined with the projector-augmented wave (PAW) method.[53] The RPBE-D3 approach was chosen as it is well suited for investigating adsorption problems.[46]

Descriptors for the CO2RR

Bagger *et al.* suggested the non-coupled gold referenced binding energies (eq. 1) of hydrogen and carbon monoxide as descriptors for electrochemical CO_2 reduction (see Ref.[34] for details):

$$\begin{aligned} \Delta E_{A^*} &= E_{Metal,A^*} - E_{Metal} - (E_{Au,A^*} - E_{Au}) + mean(\Delta E_{Au,A^*}^{\text{Gas phase}}) \\ \Delta E_{Au,A^*}^{\text{Gas phase}} &= E_{Au,A^*} - E_{Au} - E_A^{\text{Gas phase}} \end{aligned} \tag{1}$$

In their calculations they used the ensembles of 2000 energies from the Bayesian Error Estimation Functional (BEEF-vdW).[55,56] Ensembles allow for the determination of mean and standard deviation for each DFT-calculation which is why error ellipses (first σ confidence interval) for adsorption energies are obtained instead of just one point.[34] Consequently, in Eq. 1 the adsorbate is A, the ensemble consisting of 2000 energy values of the adsorbate on the metal is E_{Metal,A^*}, the metal energy ensemble is E_{Metal}, the gold reference ensemble is

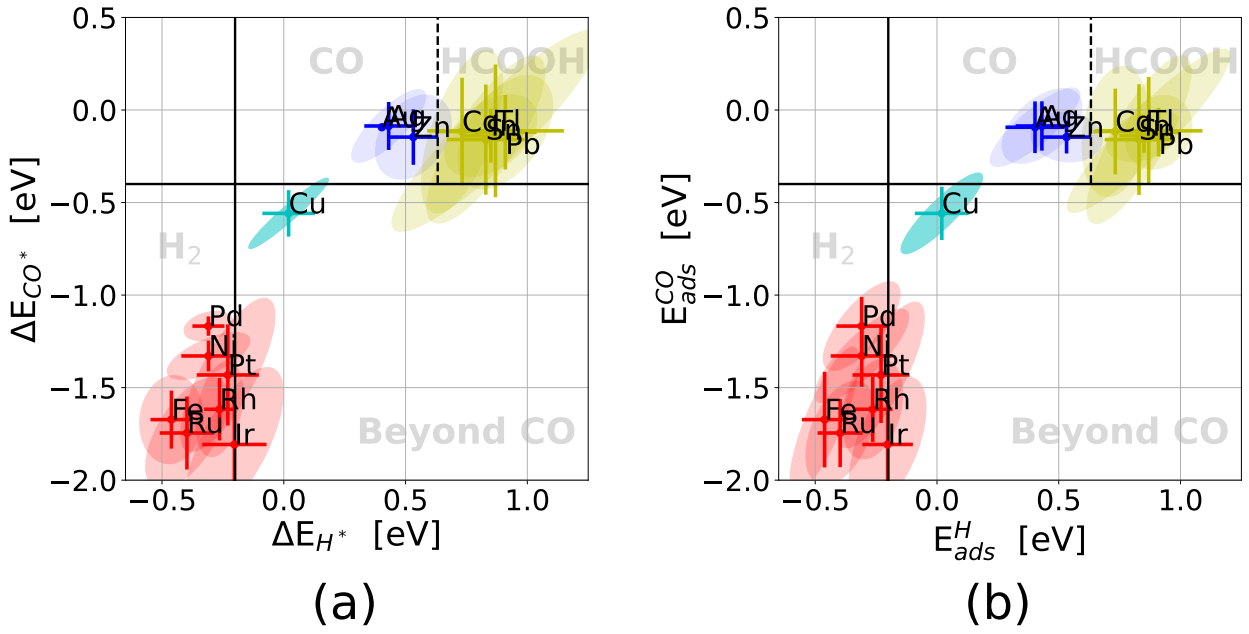


Figure 1: Comparison of plots of the data from of Bagger *et al.*[34] once evaluated with a gold reference (eq. 1) (a) and once without (eq. 15) (b).[54] Two free energy lines are drawn: horizontal signifying CO $\rightleftharpoons$ CO* with $\Delta G = 0$, and vertical signifying $\frac{1}{2}$H $\rightleftharpoons$ H* with $\Delta G = 0$, where the asterisk (*) denotes adsorption of the intermediate on the surface. The dashed line signifies the separation of carbon monoxide and formic acid as catalysis product. It is derived as being halfway between the data point for Zn and Cd. The plot has four areas H_2, CO, HCOOH and Beyond CO. Metals are grouped by the main product of CO_2 reduction with the metal as cathode, where Beyond CO stands for any hydrocarbon or alcohol.

$(E_{\mathrm{Au},A^*} - E_{\mathrm{Au}})$ and the shift by the mean binding energy on gold is $mean(\Delta E^{\text{Gas phase}}_{\mathrm{Au},A^*})$.

Using the descriptors, metals can be clustered into four categories, namely H_2, CO, HCOOH and Beyond CO. These categories refer to the main product of the CO2RR with the metal as cathode (according to the experiments of Hori *et al.*[35]), where Beyond CO in Fig. 1 stands for any hydrocarbon or alcohol.[34] Three lines separate the metals.

The vertical solid black line is constructed from the zero point energy, entropy, and heat capacity values from Chan *et al.*[57] and a correction of 0.09 eV, due to functional errors (for detail see section S2 of the Supporting Information).[58,59] The vertical solid black line marks the thermodynamics of $\frac{1}{2}H_2 \rightleftharpoons$ H* with $\Delta G = 0$. The asterisk (*) denotes adsorption of the intermediate on the surface. The line is drawn at -0.2 eV.

With respect to the vertical line in Fig. 1 identifying the equilibrium between molecular hydrogen and adsorbed atomic hydrogen we note that the original line in[34] (Bagger *et al.*) was erroneously misplaced at -0.08 eV, as also acknowledged by the authors.[60] Here we use the corrected hydrogen equilibrium line.

The horizontal solid black line is constructed from the zero point energy, entropy, and heat capacity values from Chan *et al.*[57] and a water correction for the binding energy of CO* of 0.1 eV (for detail see section S2 of the Supporting Information).[61] The horizontal solid black line marks the thermodynamics of CO $\rightleftharpoons$ CO* with $\Delta G = 0$ and is drawn at $-0.4\,\mathrm{eV}$.

The short vertical dashed black line is constructed by taking the mean H adsorption energy of Zn and Cd. This line does not have any thermodynamic interpretation attached to its derivation. To make this distinction in derivation clear the line was drawn dashed as compared to solid for the lines with thermodynamic reasoning in their derivation.

In applying these descriptors, some assumptions are made, namely: First, the metals have the same response to the electrochemical environment. Second, the information of the reaction pathway can be condensed to key binding energies. And third, although the reactions could take place on defects or kinks, considering adsorption energies of the metals (111) surface is sufficient.[34]

The assumption that the reactions do not take place on defects or kinks is not met, at least for copper. According to Scholten *et al.* surface defects, steps, and kinks are the most important catalytic sites of Cu(111) for the CO2RR.[62] That the reactions take place on special sites does not invalidate the descriptors, it just means that each unique adsorption site has to be considered when assessing a potential catalyst. Scholten *et al.* also validated experimentally that the CO adsorption energy correlates with the ability of a surface to catalyze the CO2RR.[62] The adsorption energy of carbon monoxide and hydrogen can still be used as descriptors to identify catalytic sites of interest which facilitate the CO2RR.

Workflow

In our study, we have performed DFT calculations to determine adsorption energies of hydrogen and CO on metal alloy slabs. Testing all possible unique adsorption sites requires a huge number of necessary calculations per surface slab as the number of atomic configurations and their distinct adsorption sites increases exponentially with size. To potentially reduce the number of alloy patterns for which hydrogen and carbon monoxide adsorption energies have to be examined, screening of thermodynamic stability criteria based on a workflow proposed by Xiong *et al.*,[63] was introduced.

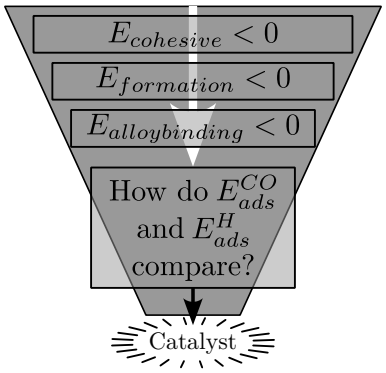


Figure 2: Workflow for systematic identification of suitable catalysts for the CO2RR. The process is based on Xiong *et al.*[63] The first three steps $E_{cohesive} < 0$, $E_{formation} < 0$, and $E_{alloybinding} < 0$ eliminate unstable surfaces. The final step compares E_{ads}^{CO} and E_{ads}^{H} following the descriptor approach of Bagger *et al.*[34]

A central quantity with respect to the stability of materials is the cohesive energy,

$$E_{cohesive} = E_{system} - \sum_{i=1}^{N_{atoms\ of\ system}} E_{atom\ i}\ . \tag{2}$$

The cohesive energy represents the energy gained when the material is formed from free atoms.

In this work we consider surface alloys, i.e., bimetallic systems in which the alloy is only formed in the first layer.[64] The formation energy can be calculated according to:

$$E_{formation} = \ E_{M1[M2]\ slab} + \ n_{rep}\ E_{M1\ atom} \ - (E_{M1\ slab} \ + n_{rep}\ E_{M2\ atom}) \tag{3}$$

Here, $M1$ denotes the bulk metal and $M2$ the dopant. $E_{M1[M2]\ slab}$ is the ground-state energy of the surface alloy slab, n_{rep} the number of $M2$ atoms, $E_{M1\ atom}$ the ground-state energy of the bulk metal $M1$ per atom; $E_{M1\ slab}$ the energy of the pure $M1$ slab, and $E_{M2\ atom}$ the ground-state energy of the bulk metal $M2$ per atom. A negative $E_{formation}$ indicates that the surface alloy formation is thermodynamically more stable than the pure $M1$ metal slab and the $M2$ atoms in their corresponding bulk structure.

The alloy binding energy is defined as:

$$E_{alloybinding} = E_{M1[M2]} - (E_{M1[-]} + n_{rep}\, E_{M2\ atom}) \tag{4}$$

Here, $E_{M1[M2]}$ is the ground-state energy of the alloy slab, $E_{M1[-]}$ is the energy of the defect slab (with dopant positions vacant), n_{rep} is the number of $M2$ atoms, and $E_{M2\ atom}$ is the bulk energy of $M2$ normalized per atom. A negative value indicates that embedding $M2$ atoms in $M1$ with a vacancy at the surface is thermodynamically favorable.

Our suggested workflow to determine adsorption energies on stable surface alloys (see Fig. 2) is divided into two parts. The first three steps assess the thermodynamic stability of the surface alloy by checking if $E_{cohesive}$, $E_{formation}$, and $E_{alloybinding}$ are all less than zero. The final step evaluates the catalytic suitability by comparing the adsorption energies of CO and H for a broad variety of adsorption sites, following the framework proposed by Bagger *et al.*[34] This approach assumes that the reaction pathway and response of the electrochemical environment of the alloy are comparable to those of the pure metals and that key adsorption energies can adequately describe catalytic activity.

Using these energetic stability criteria and the descriptors from Bagger *et al.* the suitability of four distinct copper and lead surface alloy patterns illustrated in Fig. 3 as a CO2RR catalysts was examined. These four patterns where selected because they do not form a new separate surface layer after reconstruction during relaxation. That means that the adsorption sites are of the same structure as those of the (111) surface. Therefore, available tools

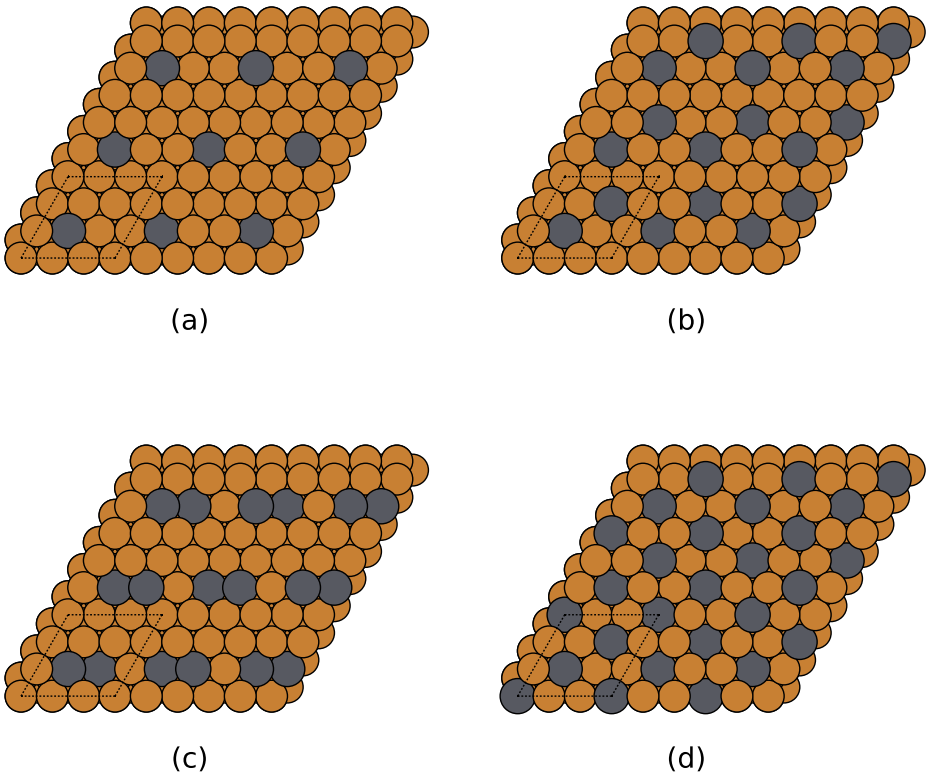


Figure 3: Starting configurations of all surface alloys chosen for the examination of adsorption energies. (a) $A_1B_8(3\times3)$/B(111), (b) $A_2B_7(3\times3)$-hex/B(111), (c) $A_2B_7(3\times3)$-dimer/B(111), $A_3B_6(3\times3)$/B(111).

for (111) surface generation and adsorbate placement can be used. This selection of patterns satisfies the restriction, that the relaxed surface can be describable as a fcc (111) surface with dopant atoms. On these surfaces, a multitude of possible adsorption sites was tested, as illustrated in section S3 of the Supporting Information. Substitution of more than three atoms for larger atoms (big radii differences) leads to reconstructions in which a new layer is formed as the original layer is too small to accommodate the bigger atoms.

Results and Discussion

Comparison of Adsorption Energies and Gold-Referenced Adsorption Energies

In a first step, we considered the particular reference used by Bagger *et al.*[34] in their determination of the adsorption energies. The descriptors proposed by Bagger *et al.* differ from standard adsorption energies by the introduction of a gold reference. They also used ensembles of adsorption energies to estimate the error of the DFT calculations. In the following, we will show that the mean of such a gold referenced ensemble is identical to the mean of

an ensemble of standard adsorption energies:

$$\bar{E} := mean(E) = \sum_{i=1}^{N} \alpha_i \; E_i \; ; \quad \sum_{i=1}^{N} \alpha_i = 1 \tag{5}$$

$$\overline{\Delta E}_{A^*} = mean\Big(E_{Metal,A^*} - E_{Metal} - (E_{Au,A^*} - E_{Au}) + mean(\Delta E^{\text{Gas phase}}_{Au,A^*})\Big) \tag{6}$$

$$= \sum_{i=1}^{N} \alpha_i \Big(E_{Metal,A^*,i} - E_{Metal,i} - (E_{Au,A^*,i} - E_{Au,i}) + \sum_{j=1}^{N} \alpha_j (\Delta E^{\text{Gas phase}}_{Au,A^*,j})\Big) \tag{7}$$

$$= \sum_{i=1}^{N} \alpha_i \Big(E_{Metal,A^*,i} - E_{Metal,i} - (E_{Au,A^*,i} - E_{Au,i})\Big) + \sum_{i=1}^{N} \alpha_i \sum_{j=1}^{N} \alpha_j (\Delta E^{\text{Gas phase}}_{Au,A^*,j}) \tag{8}$$

$$= \sum_{i=1}^{N} \alpha_i \Big(E_{Metal,A^*,i} - E_{Metal,i} - (E_{Au,A^*,i} - E_{Au,i})\Big) + \sum_{j=1}^{N} \alpha_j (\Delta E^{\text{Gas phase}}_{Au,A^*,j}) \tag{9}$$

$$= \sum_{i=1}^{N} \alpha_i \Big(E_{Metal,A^*,i} - E_{Metal,i} - (E_{Au,A^*,i} - E_{Au,i}) + \Delta E^{\text{Gas phase}}_{Au,A^*,i}\Big) \tag{10}$$

$$= mean\Big(E_{Metal,A^*} - E_{Metal} - (E_{Au,A^*} - E_{Au}) + \Delta E^{\text{Gas phase}}_{Au,A^*}\Big) \tag{11}$$

$$= mean\Big(E_{Metal,A^*} - E_{Metal} - (E_{Au,A^*} - E_{Au}) + E_{Au,A^*} - E_{Au} - E^{\text{Gas phase}}_{A}\Big) \tag{12}$$

$$= mean\Big(E_{Metal,A^*} - E_{Metal} - (E_{Au,A^*} - E_{Au}) + E_{Au,A^*} - E_{Au} - E^{\text{Gas phase}}_{A}\Big) \tag{13}$$

$$= mean\Big(E_{Metal,A^*} - E_{Metal} - E^{\text{Gas phase}}_{A}\Big) \tag{14}$$

Starting with the definition of ΔE_{A^*} (eq. 6), the mean is expressed as a weighted sum over the ensemble energies (eq. 7). The sum is then split into two terms: one dependent on index i and one independent of i (eq. 8). For the independent term, the contents can be factored out, and since $\sum_i \alpha_i = 1$, multiplication by the sum does not alter the expression

(eq. 9). The sums over i and j can be combined (eq. 10), yielding equation 11 for the mean. Inserting the definition of $\Delta E_{Au,A^*}^{\text{Gas phase}}$ (eq. 12) reveals that the gold reference cancels (eq. 13), leaving the mean of the standard adsorption energies (eq. 14).

In Fig. 1, each ellipse represents the adsorption energies for carbon monoxide and hydrogen on a specific metal. As mentioned above (section), the adsorption energy calculations are based on DFT calculations using the BEEF-vdW method. This method evaluates multiple functionals and returns an ensemble of 2000 energies. The ellipses are then generated by taking the first σ confidence interval. The mean of a given ensemble is represented by the center of the error ellipse. Therefore, if the mean does not change whether the gold reference is used or not, the ellipses center should not move when comparing Figs. 1 (a) and (b). As was proved the center does not change.

Since the gold reference does not affect the mean, it does not alter the position of the ellipses. Inclusion or exclusion of the reference however does impact the distribution of the ensemble and therefore changes the ellipse's shape. For some metals (e.g., palladium) the shape changes noticeably, while for others (e.g., copper) the change is minor. However, the clustering of metals remains unaffected (Fig. 1b). Therefore, adsorption energies can be used directly without a gold reference:

$$E_{ads}^{A} = E_{Metal,A^*} - E_{Metal} - E_{A}^{\text{Gasphase}} \tag{15}$$

In Eq. 15, A is the adsorbate, E_{Metal,A^*} the energy ensemble of the surface–adsorbate configuration, E_{Metal} the energy ensemble of clean metal surface, and E_{A}^{Gasphase} the energy ensemble of isolated adsorbate molecule. Each ensemble consists of 2000 ground-state energies. Because the gold reference does not alter the mean values and because the clustering was not affected by the exclusion of the gold reference, only adsorption energies without gold reference were used in this work.

Comparison of Copper, Lead, and Platinum results

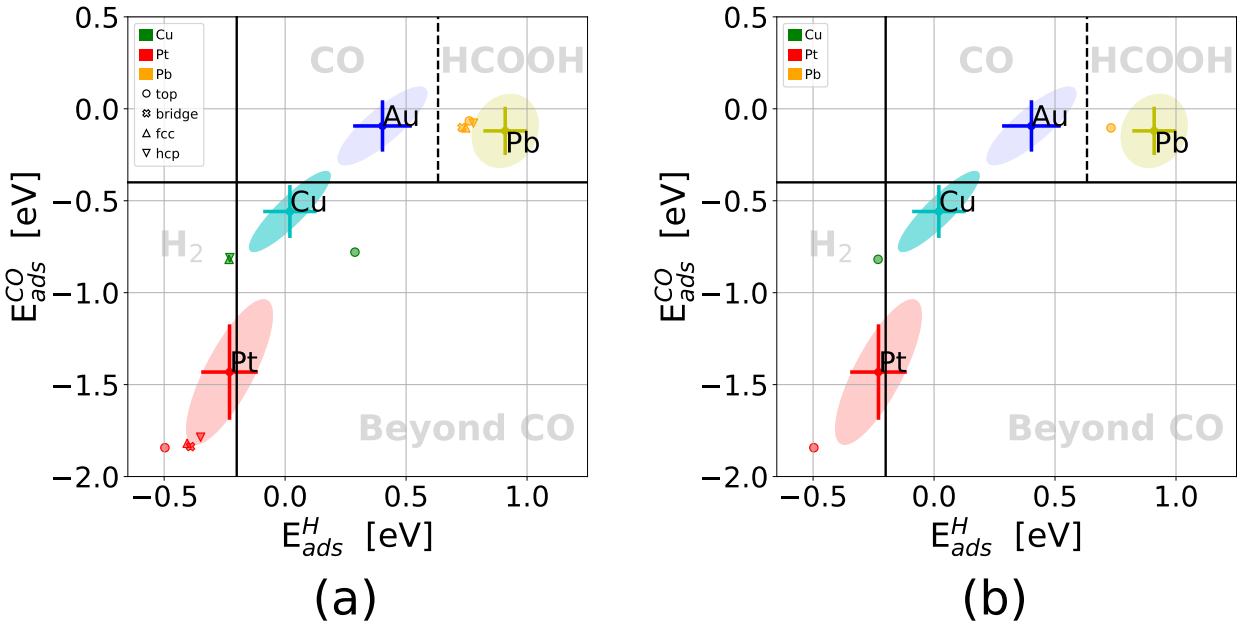


Figure 4: Adsorption energies of CO and H. Comparison of results for platinum, copper, and lead (points) with those of Bagger *et al.* for platinum, copper, gold, and lead. Panel (a) shows all adsorption energies, while panel (b) shows only the lowest-energy site combinations.

For platinum, copper, and lead (111) surfaces, adsorption energies were calculated for all sites: top, bridge, fcc, and hcp, except for the copper bridge adsorption site, as the hydrogen DFT calculation relaxed to the fcc site. In Fig. 4a, the results are plotted such that the H and CO adsorption energies for the same site are shown as a single point, e.g., hydrogen at fcc and carbon monoxide at fcc. The results are presented within the framework and dataset of Bagger *et al.* (section), which makes them easier to interpret and compare. The lowest adsorption energies correspond to the energetically most favorable sites.

For Cu, the minimum-energy sites are fcc for H and fcc for CO. The predicted CO site does not match experimental findings, where chemisorbed CO is typically observed at the top site.[65–68] However, this discrepancy is expected. DFT with local or semi-local functionals often favors the fcc site due to overestimation of back-donation to CO. Overestimated back-donation is a consequence of the underestimated HOMO–LUMO gap, which enhances interaction with surface electrons at the fcc site.[69,70] For Pt, the minimum-energy adsorption

site is top for both H and CO, consistent with experimental results for CO.[71,72] For Pb, the energetically most favorable sites are bridge for H and fcc for CO (cf. tab. 2).

The minimum-energy site combinations (e.g., H top and CO bridge for platinum) are shown in fig. 4b. Compared to Bagger *et al.*, the results fall in the same general regions: platinum in the bottom left, copper in the center and left, and lead in the top right. Platinum and lead also match with the H_2 and HCOOH groups respectively as described by Bagger *et al.*. Copper, however, falls into the H_2 group instead of the Beyond CO group. This aligns with experimental findings from Scholten *et al.*[62] who studied hydrogen adsorption on pristine and rough copper surfaces. They found that rough copper produces hydrocarbons and alcohols, whereas pristine fcc (111) surfaces of copper produce hydrogen.[62] Because pristine fcc (111) surfaces are used in DFT-calculations one would expect the results to be in the H_2 region. The RPBE-D3 method produces data points in agreement with Scholten *et al.*'s results, validating the approach.

Thermodynamic Stability of Surface Alloys

Table 1: Stability criteria for surface alloy patterns. All energies are in eV. Negative values indicate thermodynamic stability relative to the reference system; positive values indicate instability. For better comparability stability criteria are normalized. The cohesive energy is normalized to the number of atoms in the system, and the formation and alloy-binding energies are normalized to the number of dopant atoms.

structure	$\hat{E}_{formation}$	$\hat{E}_{alloybinding}$	$\hat{E}_{cohesive}$
$Pb_1Cu_8(3\times3)$/Cu(111)	-0.58	-1.19	-2.84
$Pb_2Cu_7(3\times3)$-hex/Cu(111)	-0.52	-1.15	-2.84
$Pb_2Cu_7(3\times3)$-dimer/Cu(111)	-0.38	-0.88	-2.84
$Pb_3Cu_6(\sqrt{3}\times\sqrt{3})$/Cu(111)	-0.45	-1.11	-2.84
$Cu_1Pb_8(3\times3)$/Pb(111)	0.98	0.89	-2.44
$Cu_2Pb_7(3\times3)$-hex/Pb(111)	0.85	0.71	-2.43
$Cu_2Pb_7(3\times3)$-dimer/Pb(111)	0.58	0.47	-2.44
$Cu_3Pb_6(\sqrt{3}\times\sqrt{3})$/Pb(111)	1.04	0.85	-2.41

Next, surface alloys were investigated: Pb-doped Cu and Cu-doped Pb. All four surface patterns were considered. The first three steps in the workflow examine energy criteria,

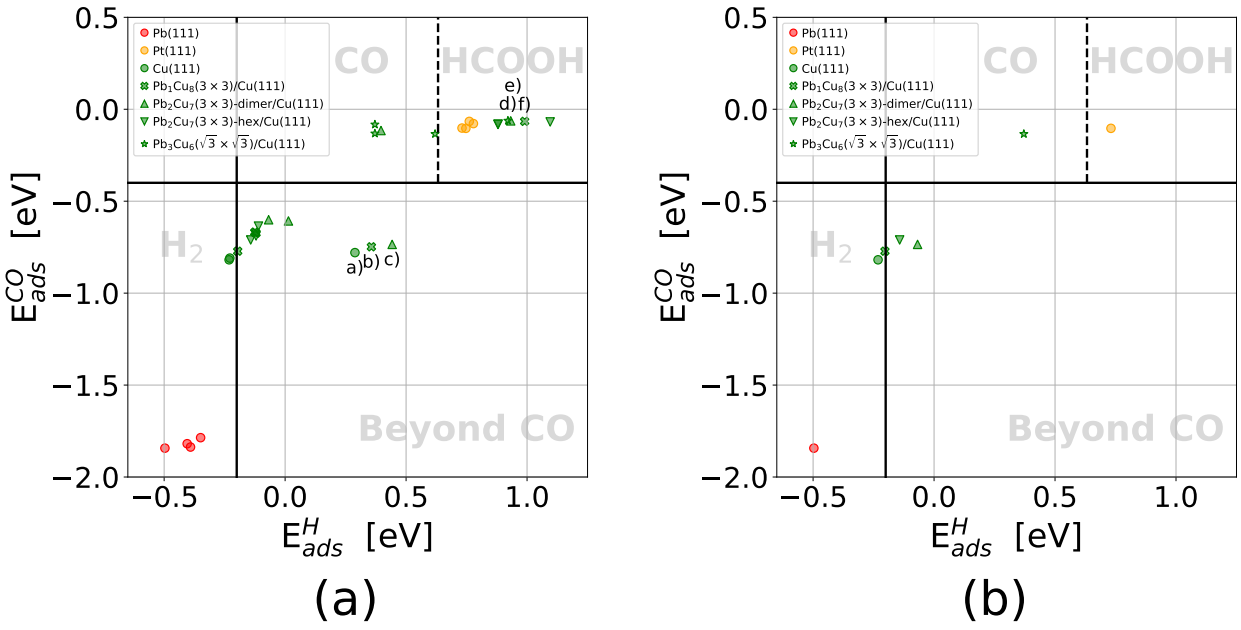


Figure 5: Adsorption energies of H and CO on Cu and Pb surface alloys and Cu, Pb and Pt metals. The copper doped with lead surface alloys are also colored green. Panel (a) shows calculations which relaxed to the same adsorption site for CO and H. Panel (b) shows only the lowest-energy site combinations.

results are summarized in Tab. 1. All PbCu surface alloy configurations on Cu(111) are thermodynamically stable with respect to the three energetic criteria, formation energy, alloy-binding energy, and cohesive energy are all negative (see Tab. 1).

In contrast, all CuPb surface alloy configurations on Pb(111) are thermodynamically unstable with respect to two of the three criteria, both the formation energy and the alloy-binding energy. Cu-doped lead alloys also exhibit a stronger surface reconstruction when adsorbates are introduced than Pb-doped copper alloys, further validating instability. Instability may arise because the smaller copper atom is less coordinated within the larger lead lattice.

Adsorption Energies on Surface Alloys

The calculated adsorption energies for H and CO on Cu, Pb, and Pt(111) surfaces and on Cu-doped Pb surface alloys are shown in Fig. 5. Each point represents two DFT calculations,

one for carbon monoxide and one for hydrogen, for which the adsorbate ended up at the same site after relaxation. Compared to the pure metals, the alloys show a much wider distribution of adsorption energies (cf. fig. 5) due to the varying chemical environments. Furthermore, generally carbon monoxide and hydrogen adsorption energies appear to correlate to a certain degree as there are no data points for the bottom right and upper left most corner.

Adsorption energies on Pb-doped Cu surfaces are spread between the adsorption energies on the clean Pb and Cu surfaces. Some sites are energetically even more unfavorable than on pure Pb. On the other hand, there are no sites produced with lower adsorption energies than on pure Cu (see the green circle in the H_2 region). This indicates that Cu surfaces alloyed with Pb atoms become less reactive.

The minimum adsorption sites are all on copper atoms (cf. tab. 2) except for the $Pb_3Cu_6(\sqrt{3} \times \sqrt{3})/Cu(111)$ pattern where a Pb atom is partially involved, as the carbon monoxide molecule is (almost) parallel to the surface (1° to surface). The adsorption on top and near the Pb atoms is unfavorable. In general, the Pb atoms appear to push all adsorbates away from where they are positioned in the surface. The adsorption on Cu atoms near Pb gets energetically less favorable compared to the pure Cu slab. In contrast, the adsorption on Pb atoms becomes energetically more favorable if further Pb atoms are introduced around it. This is illustrated in Fig. 6 where only adsorption on top sites is considered to probe the local reactivity of the metal atoms. Both the hydrogen and the CO adsorption becomes drastically less energetically favorable from the top row to the bottom row, i.e., when the adsorbates bind to Pb instead of to Cu.

The binding of CO to the surface alloy on Cu top sites becomes only slightly less favorable from a) to c) whereas for hydrogen the trend is stronger. Even smaller trends but also much weaker adsorption are observed for the H and CO adsorption on Pb top sites illustrated from d) to f). Overall these two trends are at first sight surprising as in the upper row the Pb content in the surface is increased when going from left to right whereas it is decreased in the lower row.

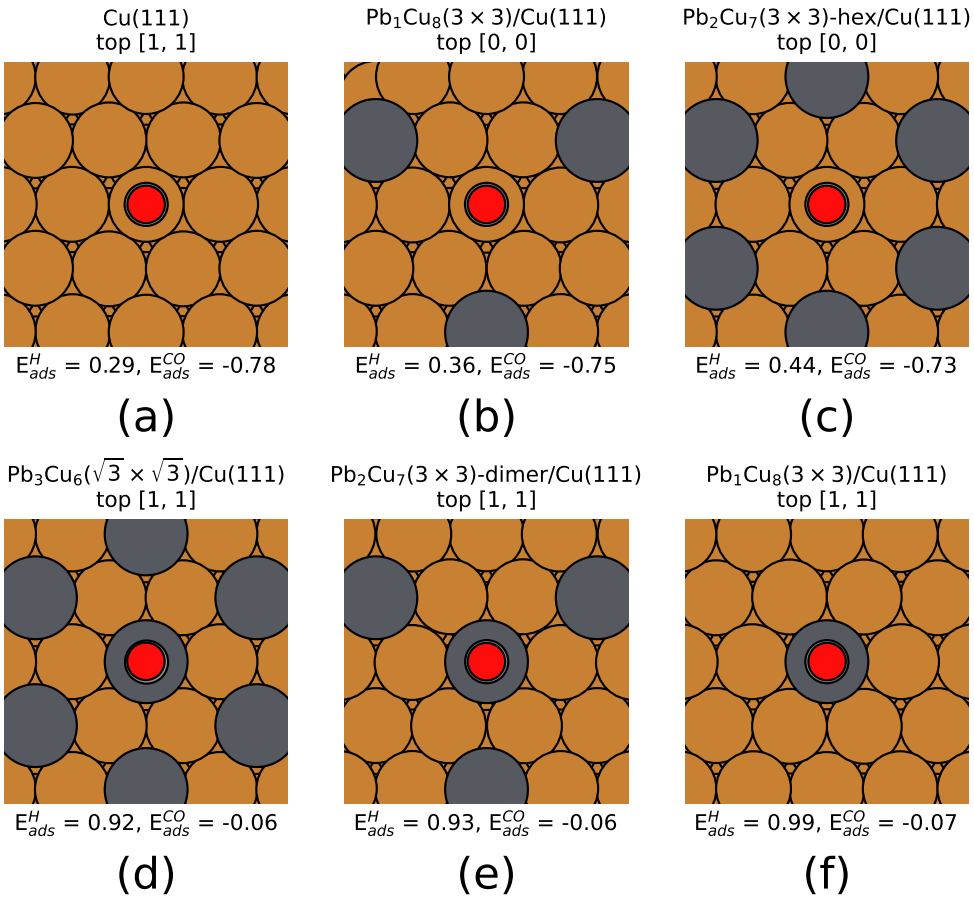
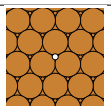
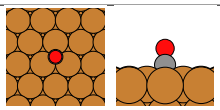
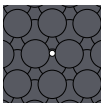
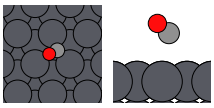
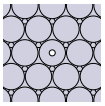
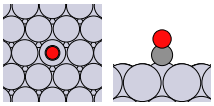
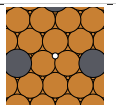
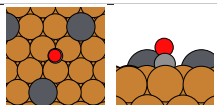
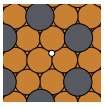
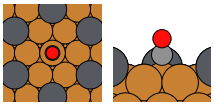
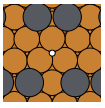
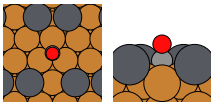
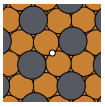
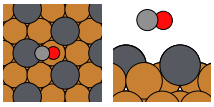


Figure 6: Selected top adsorption sites of hydrogen and CO on Pb_xCu_{9-x}/Cu(111) surface alloys for $x = 0, 1, 2, 3$. The adsorption energies in the figure that are also indicated in Fig. 5 are given in eV.

Table 2: Minimum energy adsorption sites of hydrogen (white circles) and carbon monoxide (gray and red circles) on all treated surfaces. These are the surfaces of copper (orange), platinum (light gray) lead (dark gray) and surface alloy configurations of copper and lead. All energies are in eV.

structure	H				CO			
	site	position		E_{ads}	site	position		E_{ads}
Cu(111)	fcc			-0.23	fcc			-0.82
Pb(111)	bridge			0.73	fcc			-0.10
Pt(111)	ontop			-0.50	ontop			-1.84
$Pb_1Cu_8(3\times3)/Cu(111)$	fcc			-0.20	hcp			-0.77
$Pb_2Cu_7(3\times3)$-hex/Cu(111)	fcc			-0.07	ontop			-0.73
$Pb_2Cu_7(3\times3)$-dimer/Cu(111)	fcc			-0.14	fcc			-0.71
$Pb_3Cu_6(\sqrt{3}\times\sqrt{3})/Cu(111)$	bridge			0.37	ontop			-0.13

Typically, the reactivity of bimetallic surfaces is discussed using the concepts of ligand, strain, and ensemble effects.[64,69,73] Increasing the Pb content in the first layer leads to a compressive strain effect due to the larger size of the Pb atoms which typically reduces the adsorption energies on late transition metals,[73] whereas the opposite behavior can be observed on early transition metals.[74] Furthermore, inserting a more reactive metal into a metal layer typically reduces the reactivity of the neighboring atoms as they become more strongly bound to the inserted atoms and therefore are in general less reactive due to a bond-order effect.[75] Comparing Pb and Cu, Pb is in contrast to Cu not considered to be a

noble metal but rather as a post-transition metal or a base metal, as it easily reacts with air and is prone to corrosion and oxidation. Hence, in principle both the ligand and the strain effect would predict that increasing the Pb content in a PbCu surface alloy should lead to a less strongly interacting bimetallic surface. This appears to be true for H and CO adsorption on the Cu atoms of the PbCu surface alloys, but not for H adsorption on Pb atoms. However, Pb atoms provide energetically very unfavorable adsorption sites so that they are not relevant as reaction sites. Thus, the chemical trends of Pb introduction into the surface alloy are consistent with the notion that Pb acts as a catalyst poison as it does for example in platinum car-exhaust catalysts.[76–78]

However, with respect to the selectivity of the CO2RR reflected by the descriptor, it can be noted from Fig. 5 that doping Cu with Pb pushes the adsorption energies on Cu in a direction that is desirable for a Beyond CO catalyst. Although overall the number of these adsorption sites with most favorable conditions are reduced, as some sites fall into the CO and HCOOH regions, still these overall energetically more favorable adsorption sites in the Beyond CO region are expected to dominate the CO_2 conversion as active sites. Thus, catalysts made of copper doped with lead should warrant further investigation which is also supported by experiments. Yang *et al.*[18] confirmed Cu_9Pb_1 as an CO2RR electrocatalyst with carbon monoxide and formic acid as major products. Furthermore, Wang *et al.*[37] showed that Cu/Pb (core/shell) nanocrystal catalysts can facilitate the production of C_{2+} products. These findings agree well with our results for PbCu surface alloys on copper where adsorption sites in the carbon monoxide, formic acid and Beyond CO regions where found.

Investigation of the electronic structure

Finally, we have investigated the *d*-band center of the PbCu surface alloys (see section S4 of the Supporting Information) to analyze whether the observed trends in the adsorption energy can be understood within the *d*-band model.[79,80] No significant correlation between adsorption energies and the corresponding *d*-band center was found (see Fig. S2). In fact,

this is not too surprising as the qualitative explanation for the change of the *d*-band center as a function of strain and ligand effects are in principle only applicable for d-band metals with partially filled *d*-bands[80] and not for metals with fully filled *d*-bands. This has been confirmed by electronic structure calculations for hydrogen adsorption on strained Cu surfaces in which no correlation between the position of the Cu *d*-band center and the hydrogen adsorption energies on the strained Cu surfaces has been found.[81]

Overall, the analysis suggests that while the *d*-band center remains a useful conceptual tool, it is inadequate as a quantitative descriptor for adsorption in CuPb alloys. Investigating the density of states still brought insights. According to the results shown in Fig. S2, the low-lying *d*-orbitals of Pb actually have a small bonding contribution in the CuPb/Cu(111) surface alloys.

Conclusions

In this computational study, a workflow was introduced for the systematic exploration of surface alloys as catalysts for the electrochemical CO_2 reduction reaction (CO2RR), based on the energetic stability and the suitability as a CO2RR catalyst. To check the catalytic suitability, the framework proposed by Bagger *et al.*[34] was applied which uses H and CO adsorption energies as descriptors with respect to the catalytic selectivity towards H_2, CO, HCOOH and Beyond CO (any hydrocarbon or alcohol) products of the CO2RR. First we showed that instead of the gold-referenced H and CO adsorption energies of Bagger *et al.* it is sufficient just to use standard adsorption energies.

The framework was then applied to surface alloys of copper and lead. For lead doped with copper, all tested alloy patterns were thermodynamically unstable according to the thermodynamic stability criteria inspected. In contrast, we found that doping copper with lead creates adsorption sites through a combination of strain and ligands effects that are favorable for Beyond CO products of CO_2 reduction. At the same time, other sites at these

surface alloys become more favorable for CO and HCOOH products. These computational findings align well with corresponding experimental results.

Acknowledgements

The authors acknowledge support of and many fruitful discussions with the members of the Institute of Theoretical Chemistry at Ulm University. Computer time provided by the state of Baden-Würtemberg through bwHPC and the German Research Foundation (DFG) through grant no INST 40/575-1 FUGG (Justus 2 Cluster) as well as funding through the German Bundesministerium für Forschung, Technologie und Raumfahrt (BMFTR) project NETPEC2 (grant number: 01LS2510B) and through the Dr. Babara Mez-Starck Stiftung are gratefully acknowledged.

Conflict of Interest

The authors declare no conflict of interest.

Data Availability Statement

All electronic structure calculations used in this work are made available under the Creative Commons Attribution license (CC BY 4.0) on the NOMAD (https://nomad-lab.eu) repository within the dataset https://doi.org/10.17172/nomad.sc8a-h026.

The calculated data i.e., adsorption energies, formation energies etc., plotting method and interactive figures are available on the Zenodo (https://zenodo.org/) repository https://doi.org/10.5281/zenodo.23104331.

References

(1) Horowitz, C. A. Paris Agreement. *Int. Leg. Mater.* **2016**, *55*, 740–755.

(2) May, M. M.; Rehfeld, K. ESD Ideas: Photoelectrochemical Carbon Removal as Negative Emission Technology. *Earth Syst. Dyn.* **2019**, *10*, 1–7.

(3) Anderson, K.; Peters, G. The Trouble with Negative Emissions. *Science* **2016**, *354*, 182–183.

(4) Bertone, M.; Stabile, L.; Buonanno, G. An Overview of Waste-to-Energy Incineration Integrated with Carbon Capture Utilization or Storage Retrofit Application. *Sustainability* **2024**, *16*, 4117.

(5) Supino, S.; Malandrino, O.; Testa, M.; Sica, D. Sustainability in the EU Cement Industry: The Italian and German Experiences. *J. Clean. Prod.* **2016**, *112*, 430–442.

(6) Evans, A.; Luebke, R.; Petit, C. The Use of Metal–Organic Frameworks for CO Purification. *J. Mater. Chem. A* **2018**, *6*, 10570–10594.

(7) Levi, P. G.; Cullen, J. M. Mapping Global Flows of Chemicals: From Fossil Fuel Feedstocks to Chemical Products. *Environ. Sci. Technol.* **2018**, *52*, 1725–1734.

(8) Jiang, X. Showcasing the Technological Advancements of Carbon Dioxide Conversion: A Pathway to a Sustainable Future. *RSC Sustain.* **2025**, *3*, 626–628.

(9) Wan Abdul Rahman Jauhari, W. N.; Wan Isahak, W. N. R.; Yaakob, Z. An Overview of Recent Technologies Employed for the Direct Conversion of Carbon Dioxide into Advanced Solid Materials. *Fuel* **2025**, *391*, 134620.

(10) Peterson, A. A.; Nørskov, J. K. Activity Descriptors for CO2 Electroreduction to Methane on Transition-Metal Catalysts. *J. Phys. Chem. Lett.* **2012**, *3*, 251–258.

(11) Leonzio, G.; Hankin, A.; Shah, N. CO2 Electrochemical Reduction: A State-of-the-Art Review with Economic and Environmental Analyses. *Chem. Eng. Res. Des.* **2024**, *208*, 934–955.

(12) Kirk, C.; Chen, L. D.; Siahrostami, S.; Karamad, M.; Bajdich, M.; Voss, J.; Nørskov, J. K.; Chan, K. Theoretical Investigations of the Electrochemical Reduction of CO on Single Metal Atoms Embedded in Graphene. *ACS Cent. Sci.* **2017**, *3*, 1286–1293.

(13) Siahrostami, S.; Jiang, K.; Karamad, M.; Chan, K.; Wang, H.; Nørskov, J. Theoretical Investigations into Defected Graphene for Electrochemical Reduction of CO2. *ACS Sustain. Chem. Eng.* **2017**, *5*, 11080–11085.

(14) Franco, F.; Rettenmaier, C.; Sang Jeon, H.; Cuenya, B. R. Transition Metal-Based Catalysts for the Electrochemical CO 2 Reduction: From Atoms and Molecules to Nanostructured Materials. *Chem. Soc. Rev.* **2020**, *49*, 6884–6946.

(15) Ali, A.; Qasim, M.; Sakhi, S.; Maduraiveeran, G.; Alnaser, A. S. Electrochemical CO2 Reduction: Advances, Insights, Challenges, and Future Directions. *Mater. Today Sustain.* **2025**, *30*, 101089.

(16) Yu, H.; Wu, H.; Chow, Y. L.; Wang, J.; Zhang, J. Revolutionizing Electrochemical CO2 Reduction to Deeply Reduced Products on Non-Cu-based Electrocatalysts. *Energy Environ. Sci.* **2024**, *17*, 5336–5364.

(17) Jeyachandran, N.; Yuan, W.; Giordano, C. Cutting-Edge Electrocatalysts for CO2RR. *Molecules* **2023**, *28*, 3504.

(18) Yang, S.; An, H.; Anastasiadou, D.; Xu, W.; Wu, L.; Wang, H.; de Ruiter, J.; Arnouts, S.; Figueiredo, M. C.; Bals, S.; Altantzis, T.; van der Stam, W.; Weckhuysen, B. M. Waste-Derived Copper-Lead Electrocatalysts for CO2 Reduction. *ChemCatChem* **2022**, *14*, e202200754.

(19) Esrafilzadeh, D.; Zavabeti, A.; Jalili, R.; Atkin, P.; Choi, J.; Carey, B. J.; Brkljača, R.; O'Mullane, A. P.; Dickey, M. D.; Officer, D. L.; MacFarlane, D. R.; Daeneke, T.; Kalantar-Zadeh, K. Room Temperature CO2 Reduction to Solid Carbon Species on Liquid Metals Featuring Atomically Thin Ceria Interfaces. *Nat. Commun.* **2019**, *10*, 865.

(20) Li, X.; Chen, Y.; Zhan, X.; Xu, Y.; Hao, L.; Xu, L.; Li, X.; Umer, M.; Tan, X.; Han, B.; Robertson, A. W.; Sun, Z. Strategies for Enhancing Electrochemical CO_2 Reduction to Multi-Carbon Fuels on Copper. *Innov. Mater.* **2023**, *1*, 100014.

(21) Groß, A. The Virtual Chemistry Lab for Reactions at Surfaces: Is It Possible? Will It Be Helpful? *Surf. Sci.* **2002**, *500*, 347.

(22) Chan, K.; Nørskov, J. K. Electrochemical Barriers Made Simple. *J. Phys. Chem. Lett.* **2015**, *6*, 2663–2668.

(23) Hussain, J.; Jónsson, H.; Skúlason, E. Calculations of Product Selectivity in Electrochemical CO2 Reduction. *ACS Catal.* **2018**, *8*, 5240–5249.

(24) Groß, A. Challenges in the Modeling of Elementary Steps in Electrocatalysis. *Curr. Opin. Electrochem.* **2023**, *37*, 101170.

(25) Han, J.; Bai, X.; Xu, X.; Bai, X.; Husile, A.; Zhang, S.; Qi, L.; Guan, J. Advances and Challenges in the Electrochemical Reduction of Carbon Dioxide. *Chem. Sci.* **2024**, *15*, 7870–7907.

(26) Keller, F.; Döhn, J.; Groß, A.; Busch, M. Exploring the Mechanism of the Electrochemical Polymerization of CO2 to Hard Carbon over CeO2(110). *J. Phys. Chem. C* **2024**, *128*, 6280–6293.

(27) Gholizadeh, R.; Pavlin, M.; Huš, M.; Likozar, B. Multiscale Modeling of CO2 Elec-

trochemical Reduction on Copper Electrocatalysts: A Review of Advancements, Challenges, and Future Directions. *Chemsuschem* **2025**, *18*, e202400898.

(28) Sotoudeh, M.; Groß, A. Computational Screening and Descriptors for the Ion Mobility in Energy Storage Materials. *Curr. Opin. Electrochem.* **2024**, *46*, 101494.

(29) *Computational Catalysis*; Royal Society of Chemistry, 2024.

(30) Feng, Y.; Chen, Y.; Zheng, L.; Chen, X.; Li, T.; Zhao, W. Descriptors Construction and Application in Catalytic Site Design. *iScience* **2025**, *28*, 113080.

(31) Schleder, G. R.; Padilha, A. C. M.; Acosta, C. M.; Costa, M.; Fazzio, A. From DFT to Machine Learning: Recent Approaches to Materials Science–a Review. *J. Phys. Mater.* **2019**, *2*, 032001.

(32) Klanner, C.; Farrusseng, D.; Baumes, L.; Mirodatos, C.; Schüth, F. How to Design Diverse Libraries of Solid Catalysts? *QSAR Comb. Sci.* **2003**, *22*, 729–736.

(33) Hastings, J.; Chepelev, L.; Willighagen, E.; Adams, N.; Steinbeck, C.; Dumontier, M. The Chemical Information Ontology: Provenance and Disambiguation for Chemical Data on the Biological Semantic Web. *PloS One* **2011**, *6*, e25513.

(34) Bagger, A.; Ju, W.; Varela, A. S.; Strasser, P.; Rossmeisl, J. Electrochemical CO2 Reduction: A Classification Problem. *Chemphyschem Eur. J. Chem. Phys. Phys. Chem.* **2017**, *18*, 3266–3273.

(35) Hori, Y.; Murata, A.; Takahashi, R. Formation of Hydrocarbons in the Electrochemical Reduction of Carbon Dioxide at a Copper Electrode in Aqueous Solution. *J. Chem. Soc. Faraday Trans. 1 Phys. Chem. Condens. Phases* **1989**, *85*, 2309–2326.

(36) Zheng, T.; Liu, C.; Guo, C.; Zhang, M.; Li, X.; Jiang, Q.; Xue, W.; Li, H.; Li, A.; Pao, C.-W.; Xiao, J.; Xia, C.; Zeng, J. Copper-catalysed exclusive CO_2 to pure formic acid conversion via single-atom alloying. *Nat. Nanotechnol.* **2021**, *16*, 1386–1393.

(37) Wang, P.; Yang, H.; Xu, Y.; Huang, X.; Wang, J.; Zhong, M.; Cheng, T.; Shao, Q. Synergized Cu/Pb Core/Shell Electrocatalyst for High-Efficiency CO2 Reduction to C2+ Liquids. *ACS Nano* **2021**, *15*, 1039–1047.

(38) Han, S.; Xia, W.; Jia, S.; Yao, T.; Jiao, J.; Wang, M.; Dong, X.; Yang, J.; Zhou, D.; He, M.; Wu, H.; Han, B. CO_2 Electroreduction to C_{2+} Products over Cu-Pb Heterojunction Catalyst. *ChemCatChem* **2024**, *16*, e202300918.

(39) Ma, X.; Song, X.; Zhang, L.; Wu, L.; Feng, J.; Jia, S.; Tan, X.; Xu, L.; Sun, X.; Han, B. Stabilizing Cu^0-Cu^+ sites by Pb-doping for highly efficient CO_2 electroreduction to C_2 products. *Green Chem.* **2023**, *25*, 7635–7641.

(40) Kresse, G.; Hafner, J. Norm-Conserving and Ultrasoft Pseudopotentials for First-Row and Transition Elements. *J. Phys. Condens. Matter* **1994**, *6*, 8245–8257.

(41) Kresse, G.; Furthmüller, J. Efficient Iterative Schemes Forab Initiototal-Energy Calculations Using a Plane-Wave Basis Set. *Phys. Rev. B* **1996**, *54*, 11169–11186.

(42) Kresse, G.; Joubert, D. From Ultrasoft Pseudopotentials to the Projector Augmented-Wave Method. *Phys. Rev. B* **1999**, *59*, 1758–1775.

(43) Kresse, G.; Furthmüller, J. Efficiency of Ab-Initio Total Energy Calculations for Metals and Semiconductors Using a Plane-Wave Basis Set. *Comput. Mater. Sci.* **1996**, *6*, 15–50.

(44) Hjorth Larsen, A. et al. The Atomic Simulation Environment—a Python Library for Working with Atoms. *J. Phys. Condens. Matter* **2017**, *29*, 273002.

(45) Grimme, S.; Antony, J.; Ehrlich, S.; Krieg, H. A Consistent and Accurate Ab Initio Parametrization of Density Functional Dispersion Correction (DFT-D) for the 94 Elements H-Pu. *J. Chem. Phys.* **2010**, *132*, 154104.

(46) Mahlberg, D.; Sakong, S.; Forster-Tonigold, K.; Groß, A. Improved DFT Adsorption Energies with Semiempirical Dispersion Corrections. *J. Chem. Theory Comput.* **2019**, *15*, 3250–3259.

(47) Araujo, R. B.; Rodrigues, G. L. S.; dos Santos, E. C.; Pettersson, L. G. M. Adsorption Energies on Transition Metal Surfaces: Towards an Accurate and Balanced Description. *Nat. Commun.* **2022**, *13*, 6853.

(48) Toyoda, K.; Hamada, I.; Lee, K.; Yanagisawa, S.; Morikawa, Y. Density Functional Theoretical Study of Pentacene/Noble Metal Interfaces with van Der Waals Corrections: Vacuum Level Shifts and Electronic Structures. *J. Chem. Phys.* **2010**, *132*.

(49) Granda-Marulanda, L. P.; Builes, S.; Koper, M. T. M.; Calle-Vallejo, F. Influence of van Der Waals Interactions on the Solvation Energies of Adsorbates at Pt-based Electrocatalysts. *Chemphyschem Eur. J. Chem. Phys. Phys. Chem.* **2019**, *20*, 2968–2972.

(50) Reckien, W.; Eggers, M.; Bredow, T. Theoretical Study of the Adsorption of Benzene on Coinage Metals. *Beilstein J. Org. Chem.* **2014**, *10*, 1775–1784.

(51) Monkhorst, H. J.; Pack, J. D. Special Points for Brillouin-zone Integrations. *Phys. Rev. B* **1976**, *13*, 5188–5192.

(52) Pack, J. D.; Monkhorst, H. J. "Special Points for Brillouin-zone Integrations"—a Reply. *Phys. Rev. B* **1977**, *16*, 1748–1749.

(53) Hammer, B.; Hansen, L. B.; Nørskov, J. K. Improved Adsorption Energetics within Density-Functional Theory Using Revised Perdew-Burke-Ernzerhof Functionals. *Phys. Rev. B* **1999**, *59*, 7413–7421.

(54) http://nano.ku.dk/english/research/theoretical-electrocatalysis/katladb/.

(55) Wellendorff, J.; Lundgaard, K. T.; Møgelhøj, A.; Petzold, V.; Landis, D. D.; Nørskov, J. K.; Bligaard, T.; Jacobsen, K. W. Density Functionals for Surface Science: Exchange-correlation Model Development with Bayesian Error Estimation. *Phys. Rev. B* **2012**, *85*, 235149.

(56) Medford, A. J.; Wellendorff, J.; Vojvodic, A.; Studt, F.; Abild-Pedersen, F.; Jacobsen, K. W.; Bligaard, T.; Nørskov, J. K. Assessing the Reliability of Calculated Catalytic Ammonia Synthesis Rates. *Science* **2014**, *345*, 197–200.

(57) Chan, K.; Tsai, C.; Hansen, H. A.; Nørskov, J. K. Molybdenum Sulfides and Selenides as Possible Electrocatalysts for CO2 Reduction. *ChemCatChem* **2014**, *6*, 1899–1905.

(58) Yoo, J. S.; Christensen, R.; Vegge, T.; Nørskov, J. K.; Studt, F. Theoretical Insight into the Trends That Guide the Electrochemical Reduction of Carbon Dioxide to Formic Acid. *ChemSusChem* **2016**, *9*, 358–363.

(59) Christensen, R.; Hansen, H. A.; Vegge, T. Identifying Systematic DFT Errors in Catalytic Reactions. *Catal. Sci. Technol.* **2015**, *5*, 4946–4949.

(60) Bagger, A. private communication.

(61) Peterson, A. A.; Abild-Pedersen, F.; Studt, F.; Rossmeisl, J.; Nørskov, J. K. How Copper Catalyzes the Electroreduction of Carbon Dioxide into Hydrocarbon Fuels. *Energy Environ. Sci.* **2010**, *3*, 1311–1315.

(62) Scholten, F.; Nguyen, K.-L. C.; Bruce, J. P.; Heyde, M.; Roldan Cuenya, B. Identifying Structure–Selectivity Correlations in the Electrochemical Reduction of CO2: A Comparison of Well-Ordered Atomically Clean and Chemically Etched Copper Single-Crystal Surfaces. *Angew. Chem. Int. Ed.* **2021**, *60*, 19169–19175.

(63) Xiong, B.; Yang, Y.; Liu, J.; Hua, Z.; Yang, Y. Electrocatalytic Reduction of CO2 to

C1 Products over Bimetal Catalysts: A DFT Screening Study. *Fuel Process. Technol.* **2022**, *233*, 107315.

(64) Groß, A. Tailoring the reactivity of bimetallic overlayer and surface alloy systems. *J. Phys.: Condens. Matter* **2009**, *21*, 084205.

(65) Hollins, P.; Pritchard, J. Interactions of CO Molecules Adsorbed on Cu(111). *Surf. Sci.* **1979**, *89*, 486–495.

(66) Kirstein, W.; Krüger, B.; Thieme, F. CO Adsorption Studies on Pure and Ni-covered Cu(111) Surfaces. *Surf. Sci.* **1986**, *176*, 505–529.

(67) Bönicke, I.; Kirstein, W.; Spinzig, S.; Thieme, F. CO Adsorption Studies on a Stepped Cu(111) Surface. *Surf. Sci.* **1994**, *313*, 231–238.

(68) Ammon, C.; Bayer, A.; Steinrück, H.-P.; Held, G. Low-Temperature Partial Dissociation of Water on Cu(1 1 0). *Chem. Phys. Lett.* **2003**, *377*, 163–169.

(69) Sakong, S.; Mosch, C.; Groß, A. CO Adsorption on Cu–Pd Alloy Surfaces: Ligand versus Ensemble Effects. *Phys. Chem. Chem. Phys.* **2007**, *9*, 2216–2225.

(70) Gil, A.; Clotet, A.; Ricart, J. M.; Kresse, G.; García-Hernández, M.; Rösch, N.; Sautet, P. Site Preference of CO Chemisorbed on Pt(1 1 1) from Density Functional Calculations. *Surf. Sci.* **2003**, *530*, 71–87.

(71) Baró, A. M.; Ibach, H. New Study of CO Adsorption at Low Temperature (90 K) on Pt (111) by EELS. *J. Chem. Phys.* **1979**, *71*, 4812–4816.

(72) Steininger, H.; Lehwald, S.; Ibach, H. On the Adsorption of CO on Pt(111). *Surf. Sci.* **1982**, *123*, 264–282.

(73) Mavrikakis, M.; Hammer, B.; Nørskov, J. K. Effect of strain on the reactivity of metal surfaces. *Phys. Rev. Lett.* **1998**, *81*, 2819.

(74) Schnur, S.; Groß, A. Strain and coordination effects in the adsorption properties of early transition metals: A density-functional theory study. *Phys. Rev. B* **2010**, *81*, 033402.

(75) Behm, R. J.; Groß, A. The chemistry of bimetallic surfaces - Evolution of an atomic-scale picture. *Surf. Sci.* **2025**, *754*, 122677.

(76) Thomas, V. M. The Elimination of Lead in Gasoline. *Annu. Rev. Environ. Resour.* **1995**, *20*, 301–324.

(77) Williamson, W. B.; Stepien, H. K.; Watkins, W. L. H.; Gandhi, H. S. Poisoning of Platinum-Rhodium Automotive Three-Way Catalysts by Lead and Phosphorus. *Environ. Sci. Amp Technol.* **1979**, *13*, 1109–1113.

(78) Cooper, B. J. Lead Poisoning of Automobile Emission Control Catalysts: The Influence of Emission System Design. *Platin. Met. Rev.* **1975**, *19*, 141–145.

(79) Hammer, B.; Nørskov, J. K. Electronic Factors Determining the Reactivity of Metal Surfaces. *Surf. Sci.* **1995**, *343*, 211–220.

(80) Groß, A. Adsorption at nanostructured surfaces from first principles. *J. Comput. Theor. Nanosci.* **2008**, *5*, 894.

(81) Sakong, S.; Groß, A. Dissociative adsorption of hydrogen on strained Cu surfaces. *Surf. Sci.* **2003**, *525*, 107.